

Comparison of continuous sampling with active noise cancellation and sparse sampling for cortical and subcortical auditory functional MRI

Rebecca S. Dewey^{1,2,3}   | Deborah A. Hall^{2,3,4} | Christopher J. Plack^{5,6,7} | Susan T. Francis¹

¹Sir Peter Mansfield Imaging Centre, School of Physics and Astronomy, University of Nottingham, Nottingham, United Kingdom

²National Institute for Health Research (NIHR) Nottingham Biomedical Research Centre, Nottingham, United Kingdom

³Hearing Sciences, Division of Mental Health and Clinical Neurosciences, School of Medicine, University of Nottingham, Nottingham, United Kingdom

⁴Heriot-Watt University Malaysia, Putrajaya, Malaysia

⁵Manchester Centre for Audiology and Deafness, University of Manchester, Manchester Academic Health Science Centre, Manchester, United Kingdom

⁶National Institute for Health Research Manchester Biomedical Research Centre, Central Manchester University Hospitals NHS Foundation Trust, Manchester, United Kingdom

⁷Department of Psychology, Lancaster University, Lancaster, United Kingdom

Correspondence

Rebecca Susan Dewey, National Institute for Health Research (NIHR) Nottingham Biomedical Research Centre, Nottingham NG1 5DU, United Kingdom.
Email: Rebecca.dewey@nottingham.ac.uk

Funding information

National Institute for Health Research Manchester Biomedical Research Centre; National Institute for Health Research Nottingham Biomedical Research Centre; and Medical Research Council grants awarded to the University of Manchester (MR/L003589/1 and MR/V01272X/1)

Purpose: Detecting sound-related activity using functional MRI requires the auditory stimulus to be more salient than the intense background scanner acoustic noise. Various strategies can reduce the impact of scanner acoustic noise, including “sparse” temporal sampling with single/clustered acquisitions providing intervals without any background scanner acoustic noise, or active noise cancellation (ANC) during “continuous” temporal sampling, which generates an acoustic signal that adds destructively to the scanner acoustic noise, substantially reducing the acoustic energy at the participant’s eardrum. Furthermore, multiband functional MRI allows multiple slices to be collected simultaneously, thereby reducing scanner acoustic noise in a given sampling period.

Methods: Isotropic multiband functional MRI (1.5 mm) with sparse sampling (effective TR = 9000 ms, acquisition duration = 1962 ms) and continuous sampling (TR = 2000 ms) with ANC were compared in 15 normally hearing participants. A sustained broadband noise stimulus was presented to drive activation of both sustained and transient auditory responses within subcortical and cortical auditory regions.

Results: Robust broadband noise-related activity was detected throughout the auditory pathways. Continuous sampling with ANC was found to give a statistically significant advantage over sparse sampling for the detection of the transient (onset) stimulus responses, particularly in the auditory cortex ($P < .001$) and inferior colliculus ($P < .001$), whereas gains provided by sparse over continuous ANC for detecting

This is an open access article under the terms of the Creative Commons Attribution License, which permits use, distribution and reproduction in any medium, provided the original work is properly cited.

© 2021 The Authors. *Magnetic Resonance in Medicine* published by Wiley Periodicals LLC on behalf of International Society for Magnetic Resonance in Medicine

offset and sustained responses were marginal ($p \sim 0.05$ in superior olivary complex, inferior colliculus, medial geniculate body, and auditory cortex).

Conclusions: Sparse and continuous ANC multiband functional MRI protocols provide differing advantages for observing the transient (onset and offset) and sustained stimulus responses.

KEYWORDS

auditory pathways, brainstem fMRI, functional magnetic resonance imaging, subcortical fMRI

1 | INTRODUCTION

Functional MRI (fMRI) of the auditory pathways requires a neural response to a delivered auditory stimulus that exceeds that of the scanner acoustic noise,¹ otherwise stimulus-related neuronal activity will be compromised. During image acquisition, the intense bursts of acoustic noise generated by rapidly switching the electrical current through the gradient coil generate sound-related activity in the kilohertz range, which stimulates the central auditory pathways.^{1,2} This acoustic noise confounds the detection of an fMRI response to the sound of interest, as the resting (nonstimulus periods) are never silent during conventional scanning.³ At least one study has reported that turning the coolant pumps off during acquisition can reduce some of the background scanner acoustic noise,^{4,5} but this is not a solution to the major source of acoustic noise produced by rapid gradient switching. One common approach, available on any scanner, to reduce the impact of background scanner acoustic noise is sparse temporal sampling, in which single or clustered brain volumes are acquired interspersed with periods of no data acquisition (silent period) during the stimulus presentation in a long TR.⁶⁻¹² This has been shown to enhance the detection of sound-related activity in the auditory cortex (AC) compared with more conventional continuous sampling.^{6,13} However, a sparse acquisition requires the timing of the acquisition to be well matched to the time-to-peak of the evoked fMRI hemodynamic response. This is particularly important when studying the AC, as the AC response is predominantly transient with phasic peaks in response to the onset and offset of the auditory stimulus.¹⁴ Furthermore, a sparse acquisition significantly reduces the number of fMRI acquisition volumes collected, hence altering statistical power.¹⁵ It has also been suggested that sparse temporal sampling can result in a higher number of false-positive responses than is generally acceptable.¹⁶ Determining the most favorable acquisition method for the assessment of both transient and steady-state auditory responses is paramount for studies requiring sensitivity to both cortical and subcortical activity, such as in the assessment of the effect of noise exposure on the entire ascending auditory pathway.¹⁷

An alternative approach to reduce the impact of background scanner acoustic noise is to apply active noise

cancelation (ANC). This approach is based on the principle that an additional carefully tailored acoustic signal can interfere destructively with the scanner acoustic noise, to substantially reduce the overall acoustic energy at a participant's eardrum.¹³ Active noise cancelation has been shown to improve the statistical detection of sound-related cortical activation, especially for sounds presented at low intensities.¹⁸ The benefit of ANC is that it can be used in conjunction with conventional continuous sampling, overcoming the known limitations described previously of the sparse temporal sampling. However, continuous sampling with ANC may not be as effective as sparse temporal sampling for detecting responses throughout the ascending auditory pathways.¹³

Other methods to improve the detection of auditory stimuli range from the implementation of novel acquisition techniques to reduce the background scanner acoustic noise, modification to the imaging gradients, and the presentation of auditory stimuli at higher sound levels.²⁰ This includes interleaved sparse steady state,^{15,22,23} in which the image sequence is modified such that multiple volumes (typically five) are sampled during a TR period, with a train of silent slice-selective excitation pulses used to keep the longitudinal magnetization in a steady state, or presaturated EPI using multiple delays in steady state, which uses spin saturation at a fixed delay before each volume to maintain steady-state conditions, independent of previous spin history,²⁴ and novel quiet fMRI methods based on T₂-prepared zero-TE²⁵ and Looping Star^{26,27} to reduce scanner acoustic noise. Methods of reducing the gradient noise include reducing the FOV of the imaging matrix to reduce the image readout duration and thus gradient noise,^{5,8,21} using parallel imaging for noise reduction,²⁸ decreasing the gradient slew rate to decrease the level of vibration in the gradient coil and therefore the acoustic contribution (termed "Softone"²⁹), or turning off the MR scanner coolant pump.^{4,5} More recently, the use of a multiband (MB; also called simultaneous multislice) fMRI acquisition provides a considerable reduction in the acoustic noise per unit time generated by simultaneously acquiring a given number of slices (termed the MB acceleration factor) in an imaging volume. Multiband fMRI uses MB RF pulses and parallel image reconstruction to excite multiple slices simultaneously, reducing the image acquisition train length

by the MB acceleration factor, considerably reducing the average sound level over time, with only a marginal signal-to-noise penalty if high-channel RF coils are used in combination with standard parallel imaging and MB acceleration factors.³⁰ Alternatively, the use of MB acceleration can be applied to facilitate an increase in the attainable slice coverage without increasing the acquisition time or incurring an acoustic noise penalty. De Martino et al showed that MB auditory fMRI (using an MB factor of 2 with the same coverage but a reduced acquisition time of 750 ms for MB2 compared with 1500 ms for MB1) can enhance functional responses in the AC due to lengthening the time interval between acoustic noise generated by the scanner, allowing either more silent time around the sound stimulus or for a longer sound stimulus to be presented in the longer silent interval. This resulted in significantly enhanced group-level fMRI responses ($q = 0.05$ corrected for false detection rate) to both tones and natural sounds for MB2 compared with MB1.³¹ The authors also noted that there was no significant difference in the voxel-wise temporal SNR of the MB1 and MB2 images acquired.

Methods to evaluate quantitatively the interference by background scanner acoustic noise on fMRI responses have typically been limited to the study of primary AC.^{2,3,6,13,15,16,18,19} Nevertheless, there is great interest in using fMRI to investigate sound coding throughout the central auditory pathways, including the auditory brainstem,^{5,7,8,9,10,11,20,21} as well as throughout the ascending auditory pathways.¹⁷ Here, we directly compare multiband (MB2) fMRI data collected using a sparse acquisition and continuous acquisition with ANC, acquisition schemes available on any MR vendor, for their efficacy in the detection of sound-related fMRI responses in subcortical and cortical auditory regions spanning the entire ascending auditory pathways. For this, we use amplitude modulated broadband noise stimulus to continuously stimulate both brainstem auditory nuclei and primary auditory cortex over an 18-second period. We determine whether the cortical and subcortical responses are differentially affected by the scanner acoustic noise and choice of acquisition strategy, as the primary AC response is predominantly transient, requiring sampling after stimulus onset and offset¹⁴ while subcortical structures (eg, cochlear nucleus [CN], superior olivary complex [SOC], nucleus of the lateral lemniscus [NLL] and inferior colliculus [IC], medial geniculate body [MGB]) respond to continuous sounds with a sustained fMRI response.

2 | METHODS

2.1 | Participants

Experimental procedures conformed to the World Medical Association's Declaration of Helsinki and were approved by

the University of Nottingham School of Medicine Research Ethics Committee (reference H/1408/2014/27). Fifteen participants (mean \pm SD age of 36 ± 12 years, 9 males) with self-reported normal hearing and no contraindications for MRI were recruited by advertisement across the university campus and social media.

2.2 | Functional MRI assessment

Functional MRI was used to assess sound-related responses to broadband noise across brain regions of the ascending auditory pathways, comprising the CN, SOC, NLL, IC, MGB, and AC.¹⁷ In a given scan session, the efficacy of collecting a 46 coronal oblique slice volume spanning cortical and subcortical auditory regions was compared for continuous sampling with ANC (TR = 2000 ms, with slice acquisitions equally spaced throughout the TR period) and sparse sampling (image readout duration = 1962 ms; effective TR = 9000 ms,³² with slices acquired with minimum temporal spacing in a burst at the start of the TR period). Four 10-minute fMRI runs, two sparse and two continuous ANC sampling, were collected in a randomized order across participants to control for adaptation effects. As such, habituation may have affected the results, but it is not expected to have affected one technique more than the other.

To inform placement of the slices over the ascending auditory pathways, a real-time functional localizer fMRI paradigm was first run to map responses to eight repeats of 24-second duration, 10-Hz amplitude-modulated broadband noise stimulus, generated by multiplying a broadband noise stimulus with a 10-Hz sinusoidal waveform, followed by a 40-second rest period. The amplitude-modulated stimulus is a temporally changing stimulus, and therefore drives stronger responses in the AC than broadband noise alone.

2.2.1 | Auditory stimuli

In-scanner communication, auditory stimulation, and ear protection were delivered using an OptoActive Active Noise Cancellation Headphones system (Optoacoustics, Moshav Mazor, Israel), providing passive attenuation of 24 dB. The auditory fMRI paradigm consisted of passive listening to continuous steady-state broadband noise, filtered using a first-order Butterworth filter between 1.4 kHz and 4.1 kHz, and presented at 90 dB SPL. Following an initial rest period of 20 seconds, broadband noise was presented for 18 seconds followed by a rest period of 36 seconds in a block design, with 11 repeats collected in a 614-second scan total acquisition time for each sampling scheme. A matched total acquisition time was chosen, as performed in previous comparison studies,²³ with each 614-second run consisting of 66 sparse

or 297 continuous fMRI volumes. A similar broadband noise paradigm has previously been shown to strongly drive responses in the subcortical auditory nuclei.^{14,17}

For continuous sampling only, ANC was used. To successfully compute a cancellation waveform, the ANC system required the acquisition sequence to have a TR of less than about 3 seconds. Following an initial 16-second learning period in the first of two continuous fMRI runs, ANC is reported by the manufacturer to reduce the energy of the acoustic scanner noise by approximately 35 dB (accounting for both passive and active attenuation) (https://www.optoacoustics.com/sites/default/files/documents/optoactive_brochure_2020-lite.pdf), with a similar ANC reduction being achieved at each ear in this study. This was achieved predominantly by attenuating the fundamental frequency of the scanner noise attributed to the EPI readout gradients at about 1.3 kHz, ensuring that the sound stimulus was clearly audible. During the entire 40-minute fMRI study, participants were required to attend to a fixation cross presented on a 32-inch BOLDscreen with a 1920 × 1080 widescreen liquid crystal display (Cambridge Research Systems, Rochester, United Kingdom) positioned at the rear of the scanner and viewed using a mirror attached to the head coil approximately 10 cm from the face.

2.2.2 | Functional MRI data acquisition

The fMRI data were acquired on a Philips 3T Ingenia MR scanner (Philips Healthcare, Best, Netherlands) using a 32-channel receive head coil. All data were collected using a gradient-echo EPI acquisition with 46 coronal-oblique slices of 1.5-mm isotropic spatial resolution (the orientation that provided coverage of the ascending auditory pathways [CN, SOC, NLL, IC, MGB, and AC] in the minimum volume acquisition time, FOV = of 168 × 168 × 69 mm³, TE = of 34 ms); flip angle = 90°; MB2; SENSE factor 2; and half scan (partial Fourier factor) = 0.927, with an echo spacing of 0.58 ms and bandwidth in the frequency-encoding direction of 1335 Hz, and resulting bandwidth in the phase-encoding direction of 14 Hz. This provided the necessary spatial resolution to allow assessment of the subcortical nuclei (typically < 9 mm in size³³). MB2 was chosen, as it provided sufficient slice coverage of the AC and brainstem with 1.5-mm isotropic voxels in an acceptable 2-second TR, while only marginally decreasing (~5% in AC, ~2% in brainstem) the temporal SNR compared with MB1 (Figure 1). Higher MB factors (MB3 and MB4) provide greater spatial coverage within a given volume acquisition time/TR period for sparse and continuous acquisitions. However, it can be seen that higher MB factors lead to a significant reduction in temporal SNR principally in the brainstem (MB3: 8% in AC, 35% in brainstem; MB4:

15% in AC, 51% in brainstem, as shown in Figure 1), which is problematic because fMRI responses in the brainstem are known to be lower than those in the cortex. Thus, the 46 coronal-oblique contiguous slices in the comparison study were collected in ascending order using equidistant temporal slice spacing with a TR of 2000 ms for the continuous acquisition. The sparse sampling acquisition had a 1962-ms volume acquisition time (TA) followed by a 7,038-ms silent period, resulting in an effective TR of 9000 ms, typical of previously published findings using sparse acquisitions.¹² For the continuous ANC acquisition, stimuli were synchronized with the start of the image-volume acquisition window. For the sparse acquisition, the image volume was acquired after a 6,000-ms delay from the onset/offset of the auditory stimulus, to optimally sample the hemodynamic response of the predicted transient activity in the AC. This resulted in 198/396 image volumes collected during the stimulus/rest period for the continuous ANC sampling, compared with 44/88 image volumes acquired during the stimulus/rest period for sparse sampling. Each run was preceded by preparation steps and two “dummy dynamics” for the sparse and continuous acquisitions in which no image was acquired; this allowed the tissue magnetization to reach the steady state before acquiring the image volumes during the auditory task. The breathing cycle and cardiac pulsatility were recorded throughout the fMRI acquisition using a respiratory bellow and peripheral pulse unit attached to the index finger of the left hand (Philips Healthcare, Best, Netherlands); this was used for correction of respiratory and cardiac physiological noise.

Additional EPI volumes were acquired with reversal of the fat-shift direction for image distortion correction, particularly important for alignment of the group-averaged brainstem fMRI.²¹ For accurate co-registration of the fMRI-EPI data to Montreal Neurological Institute (MNI; Montreal, Canada) standard space, a whole-brain 3D anatomical MPRAGE (TE = 2.7 ms, TR = 5.9 ms, flip angle = 8°, FOV = 168 × 168 × 164 mm³ with reconstructed voxel size 1.5 mm³) was acquired with the same spatial resolution and coronal-oblique angulation as the EPI-fMRI data.

2.2.3 | Functional MRI data preprocessing

Image preprocessing was performed using FSL software (version 6.0; FMRIB's Software Library, United Kingdom), *SPM12* software (Wellcome Trust Centre for Neuroimaging, London, United Kingdom), and in-house software coded in *MATLAB* (The MathWorks, Natick, MA). For each participant, the fMRI time-series was motion-corrected in *SPM12*, and gradient-echo EPI data were distortion-corrected using FSL's TOPUP algorithm^{34,35} and corrected for physiological noise using the respiratory and cardiac

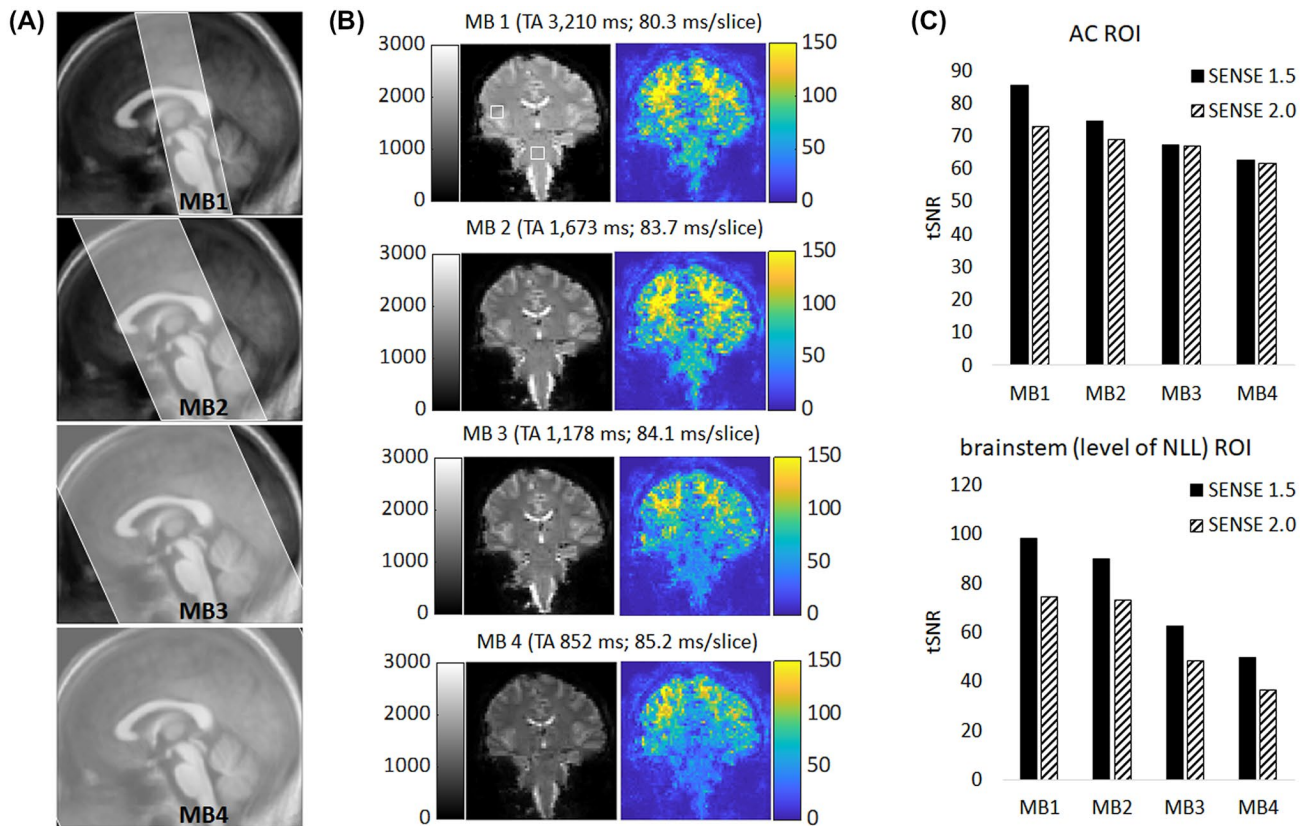


FIGURE 1 A, Illustration of the increase in slice coverage provided with increasing multiband (MB) factor of a 23-slice MB1 acquisition for MB1-MB4. B, Representative coronal slices (left; grayscale) and associated temporal SNR (tSNR) images (right; color) for images acquired using a sparse sampling scheme (TR = 9000 ms) with 2.6-mm isotropic resolution, SENSE 2, and comparable coverage (76-78 slices) across all MB factors, with volume acquisition duration (TA) provided for each. C, Associated tSNR in a 7.5-mm-cube region of interest (ROI; 125 voxels) placed in the left auditory cortex (AC; top) and brainstem at the level of the nucleus of the lateral lemniscus (NLL; bottom) computed from 20 image volumes collected at MB1-MB4 for SENSE 1.5 and SENSE 2

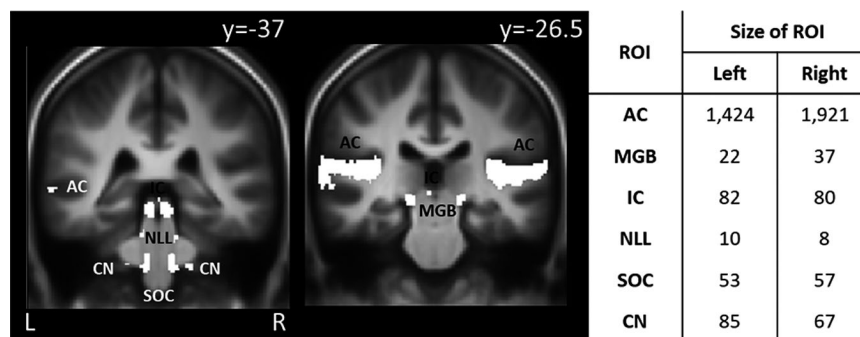


FIGURE 2 Region-of-interest definition using an entirely independent data set of 62 participants.¹⁷ The ROIs are shown in the cochlear nucleus (CN), superior olivary complex (SOC), NLL, inferior colliculus (IC), medial geniculate body (MGB) and AC, and overlaid on the group-level mean MPRAGE image (“y” denotes the Montreal Neurological Institute (MNI) slice coordinates). The table shows the number of voxels (1.5-mm isotropic) in each ROI by hemisphere

traces in RETROICOR.³⁶ Following this, data were spatially smoothed using a Gaussian kernel with a FWHM of 2 mm. Binarized masks of white matter and CSF were formed from the MPRAGE image using the segmentation tool in *SPM12* at a threshold of 0.99999. The mean time courses of white matter and CSF signal within these masks were used as covariates in the general linear model. Co-registration of

individual participant data to MNI space was performed by first realigning the distortion-corrected fMRI time series to each participant’s MPRAGE image, before co-registering to the MNI template. From this, a transformation matrix was generated that was also applied to individual statistical contrast images to facilitate group region-of-interest (ROI) analyses in MNI space.

2.2.4 | Region of interest definition

The use of anatomical landmarks or manual segmentation is challenging to define auditory brainstem and midbrain ROIs.³⁷ Instead, ROIs were defined from an independent data set formed from 62 participants, as shown in Figure 2, with the full method of ROI definition described previously.¹⁷ In brief, 62 participants were imaged using the same broadband stimulus and similar fMRI paradigm as used in the present study. Group contrast images for stimulus onset, stimulus offset, and the sustained responses were generated across all participants. These were threshold at $P < .01$ and corrected for family-wise error and binarized; a mask based on the composite (“OR” in Boolean algebra) of the three binary images was then generated. Region-specific ROIs for CN, SOC, NLL, IC, MGB, and AC were created from the anatomical definition of each subregion within this binary mask using the method of Gutschalk and Steinmann.³⁸ The use of ROI definitions taken from an independent study¹⁷ entirely avoided the issue of circularity in the analyses.³⁹

2.2.5 | Functional MRI data analysis

Data were analyzed in *SPM12* using a fixed-effects first-level analysis on individual participant’s data followed by a random-effects second-level analysis separately for the continuous ANC sampling and sparse sampling. Subsequently, comparisons were made between each sampling scheme using ROI analyses of the z-statistical maps (thus accounting for the differing number of image volumes/sample points in the two sampling schemes) and analysis of variance statistics.

The design matrix in the first-level analysis defined the explanatory variables for each individual participant as described previously.¹⁷ This consisted of the (1) transient phasic onset and offset stimulus responses, (2) sustained stimulus response, (3) six motion parameters, and (4) mean white-matter and CSF signal time-courses. In this general linear model, the phasic responses were encoded as a series of delta functions, and the sustained response was encoded as a box-car function; these were convolved with the hemodynamic response. Explanatory variables (3) and (4) were considered “nuisance” variables (ie, potential confounds in the MR signal). The fMRI time series was high pass-filtered to 1/128 Hz (twice the cycle length) and modeled for temporal autocorrelation across scans with an AR(1) process. Contrast images corresponding to stimulus onset, stimulus offset, and the sustained response were generated for each participant, and beta weights were assessed across ROIs within the ascending auditory pathways.

Data are displayed at $z = 3.29$; $P < .001$ uncorrected. Voxel-wise statistical significance is reported at $P < .05$; small volume-corrected based on independent ROIs. In

addition, the individual contrast images were interrogated to quantify the average z-score within each ROI on an individual participant basis. A repeated-measures analysis of variance was performed, with the average z-score attained using each sampling scheme (continuous ANC/sparse) within each auditory region and each stimulus response period (onset, offset, sustained) as within-subjects factors, to determine the difference in the sensitivity of the two sampling schemes and detect responses across ROIs within the ascending auditory pathways.

3 | RESULTS

3.1 | Robust sound-related responses throughout the subcortical auditory pathways

Group ($n = 15$) data showed robust sound-related activation in response to the broadband noise stimulus (Figure 3). In agreement with previous reports,^{14,40,41} the early ascending auditory pathways (CN and IC) responded predominantly with a sustained fMRI response, whereas the AC showed a strong bi-phasic response to stimulus onset and offset. The ROI time courses for CN, SOC, NLL, IC, MGB, and AC for the continuous sampling ANC scheme are shown in Figure 4. Visual inspection shows that the onset of the phasic response is more sensitive to the stimulus features than the offset, particularly for the CN, IC, and MGB, and that the sustained regressor is a poor match to the shape of the hemodynamic response in the AC compared with subcortical regions.

3.2 | Effect of sampling scheme on activity in the ascending auditory pathways

Figure 3 shows group-activation maps of the auditory pathways for continuous ANC sampling and sparse sampling. Stronger cortical responses to the stimulus onset are clearly seen for the continuous sampling scheme compared with sparse sampling; it should be noted that this accounts for the considerable increase in degrees of freedom (d.f.) of the continuous acquisition compared with sparse acquisition (570 d.f. vs 92 d.f.). Figure 5 shows the sustained response to be greater for the sparse acquisition across all ROIs, but on accounting for lower d.f. in sparse sampling this results in only a significantly greater z-score for sparse sampling in the MGB and AC. Table 1 outlines the significant responses for the sparse and continuous acquisitions to the transient (onset and offset) and sustained responses. Significant transient responses for both stimulus onset and offset were detected in the AC with continuous ANC sampling. Responses for sparse sampling had a lesser spatial extent and strength for stimulus onset and offset. For the sustained responses, clusters were

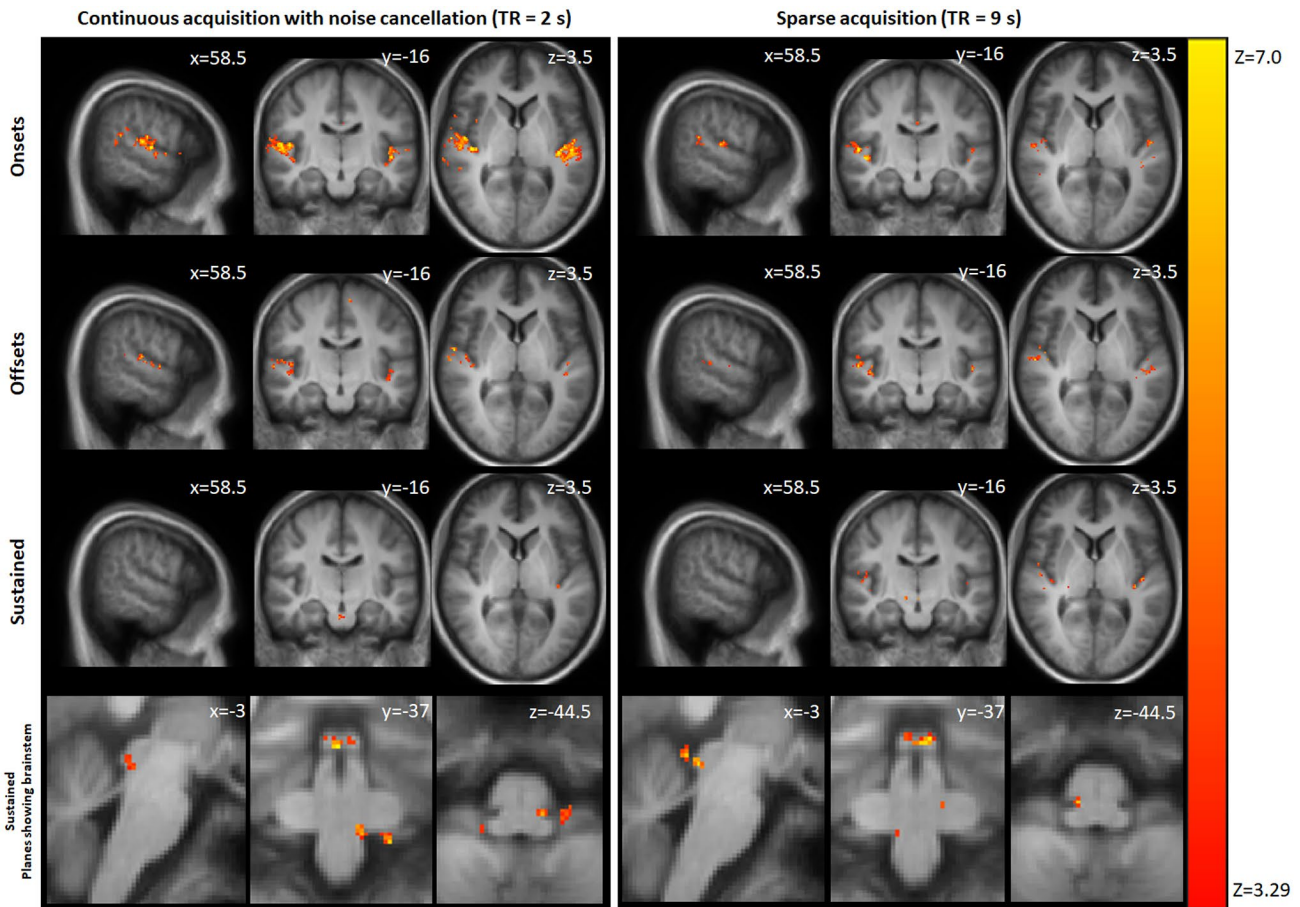


FIGURE 3 Group ($n = 15$) activation maps to onset, offset, and sustained stimulus for continuous sampling with active noise cancellation (left) and sparse sampling (right). Color bars show Z-statistic, with figures displayed at uncorrected $P < .001$ with cluster correction $k = 5$ voxels. Numbers denote the MNI slice coordinates of sagittal, coronal, and transverse images. Statistical maps are overlaid on the mean MPRAGE image. Transient responses are shown for slices $x = 58.5$, $y = -16.0$, and $z = 3.5$ mm to show the AC, while sustained responses are shown for slices $x = -3.0$, $y = 37.0$, and $z = 44.5$ mm to show the brainstem. Abbreviations: L, left; R, right

highly significant for both ACs, both ICs, and the right CN with the sparse sampling, but only significant in left AC with the continuous sampling. Clusters in right IC or AC, or in CN, SOC, NLL, and MGB did not reach statistical significance at $P < .05$ family-wise error. There was no significant effect of hemisphere using either sampling scheme ($P = .5$) and no interaction between hemisphere and either response period or sampling scheme.

Assessing data quality for the two sampling schemes, as expected, due to the longer TR of sparse sampling, image SNR was significantly higher ($P = .026$) across the ascending auditory pathway ROIs for sparse (AC, 49 ± 29 ; IC, 63 ± 37 ; CN, 48 ± 28) than continuous ANC sampling (AC, 41 ± 24 ; IC, 46 ± 28 ; CN, 39 ± 22). The temporal SNR over a fixed number of image volumes was lower for continuous sampling (sparse: AC, 30.7 ± 3.6 ; IC, 18.9 ± 2.0 ; CN, 15.3 ± 2.0 ; continuous ANC: AC, 27.9 ± 3.3 ; and continuous ANC: IC, 16.8 ± 1.9 ; CN, 14.2 ± 1.5 ; $P = .027$); however, this is counteracted by greater statistical power from more samples per unit time for the continuous sampling scheme.

3.3 | Assessment of responses using ROI analysis

Because there was no significant effect of hemisphere, ROI analysis was performed combined across hemispheres. Figure 5 shows the fMRI mean z-score in each ROI (CN, SOC, NLL, IC, MGB, and AC) for both sparse and continuous with ANC sampling schemes. When assessed for their similarity to a normal distribution, there was no significant degree of skew or kurtosis in any ROI at a level of $P < .01$, so an analysis of variance was subsequently used to interrogate these metrics.

Analysis of variance statistics on the mean z-score in each ROI showed a significant effect of response period ($F = 20.30$; d.f. = 2, 28; $P < .001$) and ROI ($F = 33.42$; d.f. = 5, 70; $P < .001$) but not sampling scheme ($F = 0.01$; d.f. = 1, 14; $P = .9$). There were significant interactions for response period*sampling scheme ($F = 30.78$; d.f. = 2, 28; $P < .001$) and ROI*response period ($F = 12.34$; d.f. = 10, 140; $P < .001$), but not for ROI*sampling scheme ($F = 0.75$;

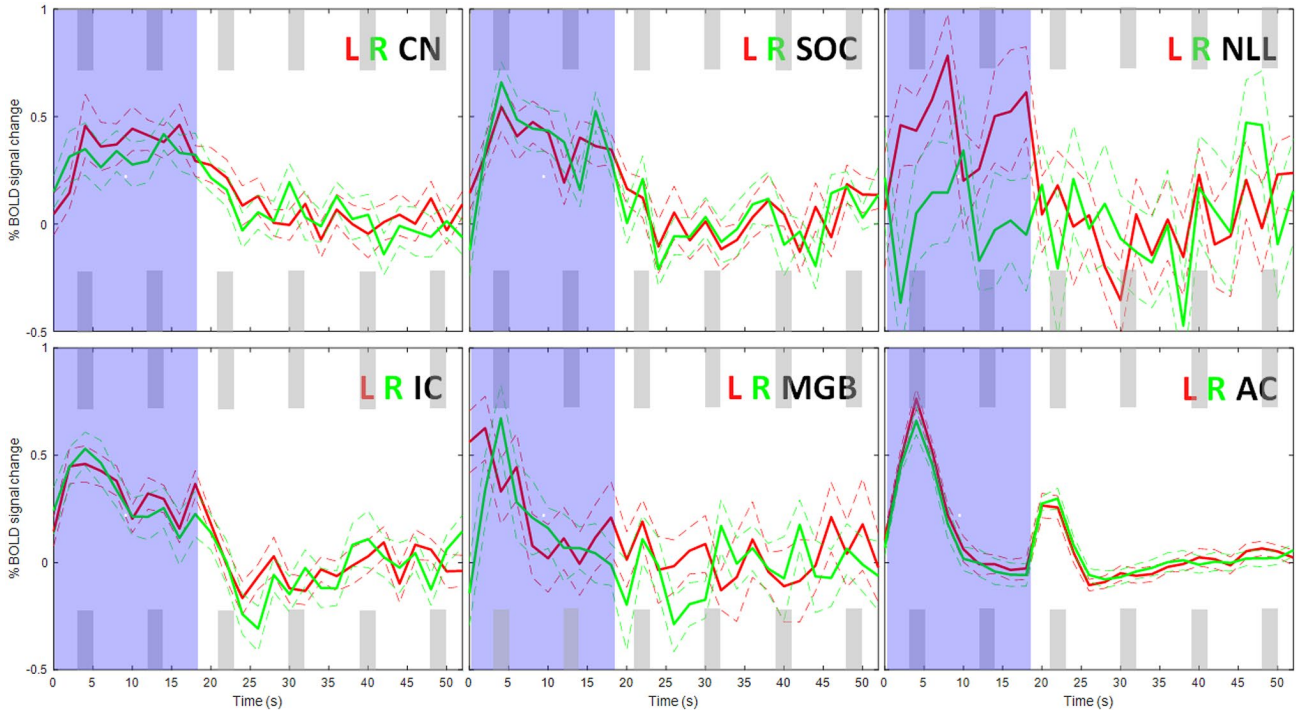


FIGURE 4 Group mean BOLD percentage change to broadband noise stimulation (all participants, $n = 15$) in the CN, SOC, NLL, IC, MGB, and AC ROIs, as acquired using the continuous ANC sampling scheme. Dashed lines show the standard error. Note the systematic variation in the functional MRI (fMRI) response to the broadband noise stimulus epoch throughout the auditory pathways from one that is sustained over the stimulus epoch (CN, SOC, NLL, and IC) to one that is phasic at stimulus onset and offset (MGB and AC). Blue shading represents the timing and duration of the broadband noise stimulus. Gray bars indicate the 1962-ms sparse image volume acquisitions. Abbreviations: L, left; R, right

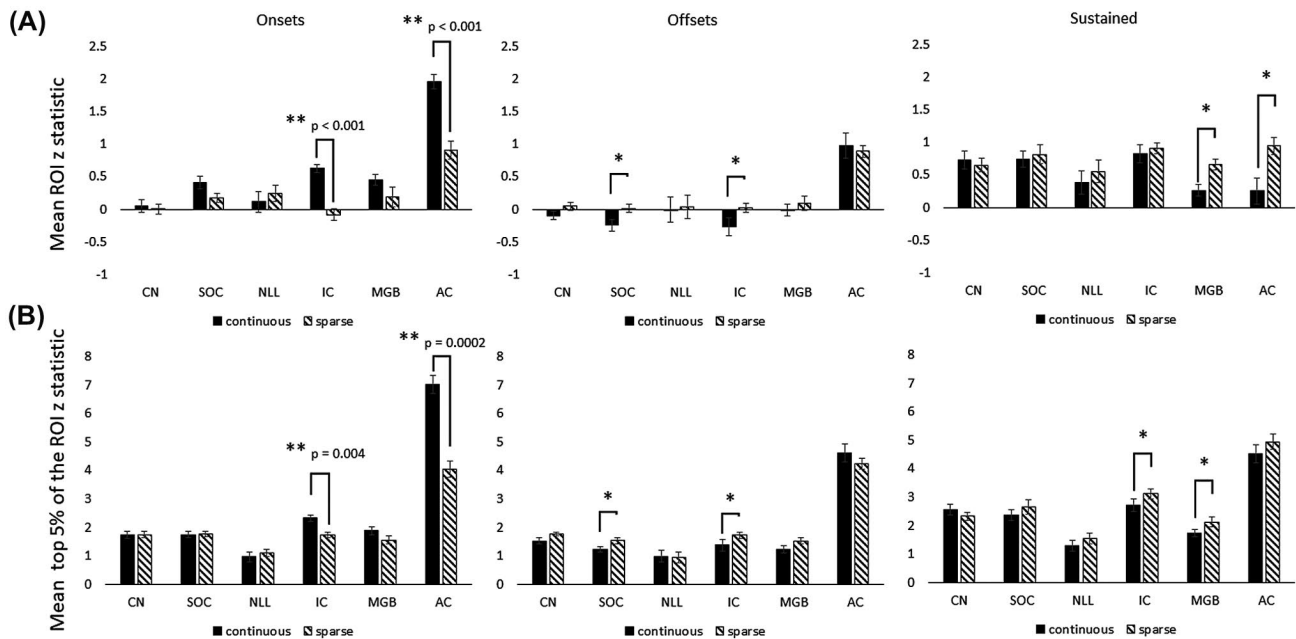


FIGURE 5 A, Mean z-statistics in the ROI for the onset, offset, and sustained fMRI response (and associated standard error) for continuous and sparse fMRI sampling schemes across the group ($n = 15$). B, Mean of the top 5% of the voxel z-statistics in the ROI shown for onset, offset, and sustained fMRI response using the continuous and sparse sampling schemes across the group ($n = 15$). For each, * denotes a significant difference in sampling scheme at $P < .05$ when corrected for multiple comparisons using a two-stage linear step-up procedure of Benjamini, Krieger, and Yekutieli; ** denotes significance at the level quoted after Bonferroni correction

TABLE 1 Significant responses for the sparse and continuous acquisitions to the transient (onset and offset) and sustained responses for voxel-wise statistical significance reported at $P < .05$ and small volume-corrected based on independent ROIs

Sparse	Region	Hemisphere	z	k	P (FWE)
Onset	AC	L	4.47	87	<.001
		R	4.82	248	<.001
Offset		L	4.51	358	<.001
		R	4.59	156	<.001
Sustained		L	5.37	231	<.001
		R	5.27	195	<.001
	IC	L	4.38	49	<.001
		R	4.72		<.001
	CN	R	4.19	0.044	.044
Continuous	Region	Hemisphere	z	k	P (FWE)
Onset	AC	R	5.43	1136	<.001
		L	5.78	1832	<.001
Offset	AC	R	4.41	291	<.001
		L	4.24	102	<.001
Sustained	AC	L	4.66	35	<.001
	IC	L	4.04	29	<.001

Abbreviation: FWE, family-wise error.

d.f. = 5, 70; $P = .1$), demonstrating that neither sampling scheme was preferable for studying fMRI response in the entire auditory pathways. There was a significant interaction ROI*response period *sampling scheme ($F = 10.26$; d.f. = 10, 140; $P < .001$), suggesting that the degree of benefit afforded by using one sampling scheme over the other varied across the ascending auditory pathways. Post hoc Student's t-tests (indicated by * and ** in Figure 5A) showed that the effect of sampling scheme was largely driven by greater responses in AC and MGB for the sustained stimulus response and greater onset responses in AC and MGB for continuous sampling. There was no consistent significant difference between the fMRI responses measured using continuous ANC and sparse sampling in subcortical regions for the transient stimulus responses.

Due to the ROI size varying substantially across the auditory pathways (subcortical ROIs ranging in size from 8 to 85 voxels, compared with each AC ROI containing over 1000 voxels), the ROI analyses were also computed using the top 5% of active voxels in each ROI, as opposed to the mean of all voxels in the ROI (Figure 5B). This secondary analysis again showed a significant effect of response period ($F = 21.15$; d.f. = 2, 28; $P < .001$) and ROI ($F = 206.51$; d.f. = 5, 70; $P < .001$) but not sampling scheme ($F = 1.34$; d.f. = 1, 14; $P = .3$), confirming that neither sampling scheme was preferable for all ROIs in the entire auditory pathways. There were significant interactions for response period*sampling scheme ($F = 34.32$; d.f. = 2, 28; $P < .001$) and ROI*stimulus ($F = 9.40$; d.f. = 10, 140; $P < .001$). There was also a significant

interaction for the ROI*sampling scheme ($F = 10.15$; d.f. = 5, 70; $P < .001$), which suggests that, when considering just the most active voxels in each ROI, the most effective sampling scheme differed with ROI. There was once again a significant interaction ROI* response period*sampling scheme ($F = 5.60$; d.f. = 10, 140; $P < .001$). Bonferroni-corrected post hoc Student's t-tests once again showed that the onset responses in AC and IC were best sampled using a continuous sampling strategy; the offset response was best sampled in the IC and SOC by sparse sampling; and the sustained stimulus response was optimally sampled by the sparse scheme in IC and MGB (Figure 5B).

4 | DISCUSSION

This study sought to evaluate continuous sampling with commercially available ANC against sparse sampling, both with the use of MB2 acquisition, to study the hemodynamic responses to a broadband noise stimulus in the ascending auditory pathways.

4.1 | Effect of sampling scheme

The higher temporal sampling of continuous ANC was found to be superior to sparse sampling for the detection of the transient onset responses dominant in the AC and IC. Sparse sampling gave some advantages over continuous ANC in

detecting offset and sustained responses throughout the ascending auditory pathways.

A truly continuous scanner acoustic noise will be much less stimulating to cortical regions (AC and MGB) due to its unchanging nature. This was demonstrated in the study of Sefritz et al,⁴² who compared conventional continuous fMRI with a “modified” continuous fMRI scheme, dividing the EPI readout train into 10 blocks to generate a perceptually more continuous acoustic noise. They show a greater response to the “modified continuous” compared with “conventional continuous” response in the auditory cortex and MGB. However, a continuous stimulus will still present a significant confound to the assessment of subcortical responses due to the total acoustic energy presented as compared with sparse fMRI. We believe that the sound produced by continuous scanning itself, even at a level reduced through the use of ANC, is enough to drive activity in these lower auditory structures, and can lead to an elevated baseline in the “silent” rest condition. We propose that this translates into the reduced activity detectable by the general linear model analysis for the continuous compared with sparse acquisition, and this interpretation is supported by the *z*-scores to sustained responses (see Figure 5). Another contributing factor may be that of forward suppression, which plays a role in reducing the neural response to subsequent bursts following the initial stimulus burst.^{14,43}

Continuous sampling provides the advantage of a greater number of time points per unit time, allowing good sampling of transient onset responses, albeit with higher acoustic noise, and results in a higher d.f. and therefore sensitivity than sparse for a given neural response. In contrast, careful implementation of timings is critical for the sparse sampling, as the sensitivity to detect onset responses is highly dependent on timing the acquisition to occur concurrently with the peak of the stimulus response, and an appropriate TR and stimulus length must be chosen to also sample the stimulus offset. As explained in previously published work,^{13,18} gains in the sustained response for sparse sampling can be explained by both the reduced interference of scanner acoustic noise (here the 9000-ms TR comprised only 1962 ms of scanner acoustic noise during the MB2 acquisition, with the remaining 7038 ms of either stimulus or silence, and by increases in the image and temporal SNR due to full T_1 recovery between volume acquisitions as compared with the 2000-ms TR of the continuous ANC sequence). It was shown that the effect size (b) to the sustained response was greater for the sparse sampling, although this was traded against statistical power being reduced due to fewer samples per unit time. Given this, it will be of interest in the future to assess the benefits of a clustered sparse sampling method, accounting for the increased total acquisition time (see section 4.3).

4.2 | Choice of auditory stimulus, sampling schemes, and postprocessing

Here, a continuous broadband stimulus was selected to stimulate activity throughout the central auditory pathways, in both brainstem auditory nuclei and the AC. A broadband noise stimulus was chosen, as the lower regions of the pathways (CN, SOC, NLL, and IC) are known to respond more to sustained acoustic energy.¹⁴ In a previous study,¹³ we showed that ANC has a substantial benefit for speech perception and comprehension presented in the MR scanner, greater than for sparse imaging alone. In that study, ANC was rated by listeners as advantageous for clarity, listening effort, and background noise intrusion, with no statistical difference in ratings between speech and broadband noise stimuli. However, we acknowledge that ANC does have some limitations, especially for contrasts between stimuli with substantial high-frequency content, in which ANC is least effective such as speech stimuli.

A fixed TR was used for both the continuous and sparse sampling. Potentially, fMRI of the brainstem can be confounded by artifacts caused by cardiac-related, pulsatile brainstem motion (ie, the brainstem moves with each arterial pulsation).²¹ Here we performed RETROICOR to address this effect. An alternative solution is cardiac gating of images, in which the image acquisition is synchronized to a given point of the subject’s cardiac cycle. However, because the heart rate naturally varies beat to beat, this results in a nonconstant TR that varies with heartrate, a significant confound. Guimaraes et al²¹ proposed a postacquisition correction adjusting for such interimage variations in the signal intensity caused by a varying TR,⁴⁴ and has been shown to improve detection of fMRI responses in the colliculi and cortex.^{4,5,8,20,21,45,46,47}

The ROIs of the ascending auditory pathways were derived from an entirely independent data set,¹⁷ thus precluding any form of circularity in the analysis.³⁹ Because these ROIs varied substantially in size, with subcortical ROIs ranging in size from 8 to 85 voxels and AC ROIs over 1000 voxels each, ROI analyses are also shown for the top 5% of active voxels in each ROI, in addition to the conventional approach of mean of all voxels in the ROI. Furthermore, this approach of studying the top 5% of active voxels accounts for the wide anatomical variation in functionally responsive areas between participants, and the potential that the mean is not representative of the active voxels for small brain regions such as brainstem subcortical structures.

4.3 | Future directions

Some success has been demonstrated using subcortical auditory fMRI at a field strength of 7 T,⁴⁸ providing improvements in sensitivity in the single subject necessary for

high-resolution mapping of the subcortical substructure. However, the “lower” field strength of 3 T, as used in this study, is far more widely available, financially accessible, and better tolerated by patients, particularly those experiencing symptoms of auditory disorders such as tinnitus and hyperacusis or reduced sound-level tolerance.

More recently, some functional subcortical studies at 3 T and 7 T have used a clustered sparse acquisition with a TR of between 2000 and 2800 ms.⁴⁸⁻⁵³ This approach has the added advantage of being able to better sample the transient BOLD responses.³³ However, clustered sparse acquisitions require the rapid acquisition of the imaging volumes to ensure there is a sufficiently long silent period in which the stimulus is presented.¹⁵ The implementation of such a clustered approach can be limited when a high number of slices are acquired, as when high spatial resolution is required to sampling the whole ascending auditory pathways. Here, we used MB2 to reduce the volume acquisition time to the order of 2000 ms. Further increasing the MB factor will reduce the image volume acquisition time for such a clustered approach, but as shown in Figure 1, it would come at the cost of temporal SNR, particularly in the brainstem. Future studies will assess the impact of jittered sparse or clustered sparse with a sufficient silent period on functional contrast to maximize both cortical and brainstem responses. This would have the advantage of full temporal sampling of the hemodynamic response curve. However, the statistical power over the time course would be weaker, as each point would be sampled fewer times, which may limit the assessment of transient responses. To compensate for this, additional fMRI runs may be required.

5 | CONCLUSIONS

Widely available sparse and continuous ANC MB fMRI sampling protocols provide differing advantages for observing the transient (onset and offset) and sustained stimulus response dependent on the level of the region in the ascending auditory pathways. Overall, for a matched total acquisition time, continuous ANC gave advantages over sparse for detecting transient (onset) responses particularly in AC, whereas gains provided by sparse over continuous ANC were marginal for detecting offset and sustained responses throughout the ascending auditory pathways.

ORCID

Rebecca S. Dewey  <https://orcid.org/0000-0002-6888-3298>

TWITTER

Rebecca S. Dewey  @rebecca_penguin

REFERENCES

1. Ravicz ME, Melcher JR, Kiang NY. Acoustic noise during functional magnetic resonance imaging. *J Acoust Soc Am.* 2000;108:1683-1696.
2. Hall DA, Summerfield AQ, Gonçalves MS, et al. Time-course of the auditory BOLD response to scanner noise. *Magn Reson Med.* 2000;43:601-606.
3. Scarff CJ, Dort JC, Eggermont JJ, et al. The effect of MR scanner noise on auditory cortex activity using fMRI. *Hum Brain Mapp.* 2004;22:341-349.
4. Melcher JR, Levine RA, Bergevin C, et al. The auditory midbrain of people with tinnitus: abnormal sound-evoked activity revisited. *Hear Res.* 2009;257:63-74.
5. Hawley ML, Melcher JR, Fullerton BC. Effects of sound bandwidth on fMRI activation in human auditory brainstem nuclei. *Hear Res.* 2005;204:101-110.
6. Hall DA, Haggard MP, Akeroyd MA, et al. “Sparse” temporal sampling in auditory fMRI. *Hum Brain Mapp.* 1999;7:213-223.
7. Gu JW, Halpin CF, Nam E-C, et al. Tinnitus, diminished sound-level tolerance, and elevated auditory activity in humans with clinically normal hearing sensitivity. *J Neurophysiol.* 2010;104:3361-3370.
8. Melcher JR, Sigalovsky IS, Guinan JJ, et al. Lateralized tinnitus studied with functional magnetic resonance imaging: abnormal inferior colliculus activation. *J Neurophysiol.* 2000;83:1058-1072.
9. Lanting CP, De Kleine E, Bartels H, et al. Functional imaging of unilateral tinnitus using fMRI. *Acta Otolaryngol.* 2008;128:415-421.
10. Lanting CP, de Kleine E, Langers DRM, et al. Unilateral tinnitus: changes in connectivity and response lateralization measured with fMRI. *PLoS One.* 2014;9:e110704.
11. Slabu LM. The effect of slice orientation on auditory FMRI at the level of the brainstem. *Brain Topogr.* 2010;23:301-310.
12. Perrachione TK, Ghosh SS. Optimized design and analysis of sparse-sampling FMRI experiments. *Front Neurosci.* 2013;7:55.
13. Blackman GA, Hall DA. Reducing the effects of background noise during auditory functional magnetic resonance imaging of speech processing: qualitative and quantitative comparisons between two image acquisition schemes and noise cancellation. *J Speech Lang Hear Res.* 2011;54:693-704.
14. Harms MP, Melcher JR. Sound repetition rate in the human auditory pathway: representations in the waveshape and amplitude of fMRI activation. *J Neurophysiol.* 2002;88:1433-1450.
15. Schwarzbauer C, Davis MH, Rodd JM, et al. Interleaved silent steady state (ISSS) imaging: a new sparse imaging method applied to auditory fMRI. *Neuroimage.* 2006;29:774-782.
16. Manno FAM, Fernandez-Ruiz J, Manno SH, Cheng SH, Lau C, Barrios FA. Sparse sampling of silence type I errors with an emphasis on primary auditory cortex. *Front Neurosci.* 2019;13:516.
17. Dewey RS, Francis ST, Guest H, et al. The association between subcortical and cortical fMRI and lifetime noise exposure in listeners with normal hearing thresholds. *Neuroimage.* 2020;204:116239.
18. Hall DA, Chambers J, Akeroyd MA, et al. Acoustic, psychophysical, and neuroimaging measurements of the effectiveness of active cancellation during auditory functional magnetic resonance imaging. *J Acoust Soc Am.* 2009;125:347-359.
19. Hall DA, Haggard MP, Summerfield AQ, et al. Functional magnetic resonance imaging measurements of sound-level encoding in the absence of background scanner noise. *J Acoust Soc Am.* 2001;109:1559-1570.

20. Sigalovsky IS, Melcher JR. Effects of sound level on fMRI activation in human brainstem, thalamic and cortical centers. *Hear Res.* 2006;215:67-76.
21. Guimaraes AR, Melcher JR, Talavage TM, et al. Imaging subcortical auditory activity in humans. *Hum Brain Mapp.* 1998;6:33-41.
22. Andoh J, Ferreira M, Leppert IR, et al. How restful is it with all that noise? Comparison of Interleaved silent steady state (ISSS) and conventional imaging in resting-state fMRI. *Neuroimage.* 2017;147:726-735.
23. Mueller K, Mildner T, Fritz T, et al. Investigating brain response to music: a comparison of different fMRI acquisition schemes. *Neuroimage.* 2011;54:337-343.
24. Shrestha M, Lee HS, Nöth U, et al. A novel sequence to improve auditory functional MRI with variable silent delays. *Magn Reson Med.* 2021;85:883-896.
25. Solana AB, Menini A, Sacolick LI, Hehn N, Wiesinger F. Quiet and distortion-free, whole brain BOLD fMRI using T2-prepared RUFIS. *Magn Reson Med.* 2016;75:1402-1412.
26. Wiesinger F, Menini A, Solana AB. Looping star. *Magn Reson Med.* 2019;81:57-68.
27. Dionisio-Parra B, Wiesinger F, Sämann PG, et al. Looping star fMRI in cognitive tasks and resting state. *J Magn Reson Imaging.* 2020;52:739-751.
28. Dezwart J, Vangelder P, Kellman P, et al. Reduction of gradient acoustic noise in MRI using SENSE-EPI. *Neuroimage.* 2002;16:1151-1155.
29. Rondinoni C, Amaro Jr E, Cendes F, et al. Effect of scanner acoustic background noise on strict resting-state fMRI. *Braz J Med Biol Res.* 2013;46:359-367.
30. Barth M, Breuer F, Koopmans PJ, et al. Simultaneous multislice (SMS) imaging techniques. *Magn Reson Med.* 2016;75:63-81.
31. De Martino F, Moerel M, Ugurbil K, et al. Less noise, more activation: multiband acquisition schemes for auditory functional MRI. *Magn Reson Med.* 2015;74:462-467.
32. Langers DRM, Sanchez-Panchuelo RM, Francis ST, et al. Neuroimaging paradigms for tonotopic mapping (II): the influence of acquisition protocol. *Neuroimage.* 2014;100:663-675.
33. Ress D, Chandrasekaran B. Tonotopic organization in the depth of human inferior colliculus. *Front Hum Neurosci.* 2013;7:586.
34. Smith SM, Jenkinson M, Woolrich MW, et al. Advances in functional and structural MR image analysis and implementation as FSL. *Neuroimage.* 2004;23:S208-S219.
35. Andersson JL, Skare S, Ashburner J. How to correct susceptibility distortions in spin-echo echo-planar images: application to diffusion tensor imaging. *Neuroimage.* 2003;20:870-888.
36. Glover GH, Li TQ, Ress D. Image-based method for retrospective correction of physiological motion effects in fMRI: RETROICOR. *Magn Reson Med.* 2000;44:162-167.
37. Devlin JT, Sillery EL, Hall DA, et al. Reliable identification of the auditory thalamus using multi-modal structural analyses. *Neuroimage.* 2006;30:1112-1120.
38. Gutschalk A, Steinmann I. Stimulus dependence of contralateral dominance in human auditory cortex. *Hum Brain Mapp.* 2015;36:883-896.
39. Kriegeskorte N, Simmons WK, Bellgowan PSF, et al. Circular analysis in systems neuroscience: the dangers of double dipping. *Nat Neurosci.* 2009;12:535-540.
40. Giraud A-L, Lorenzi C, Ashburner J, et al. Representation of the temporal envelope of sounds in the human brain. *J Neurophysiol.* 2000;84:1588-1598.
41. Nourski KV, Brugge JF. Representation of temporal sound features in the human auditory cortex. *Rev Neurosci.* 2011;22:187-203.
42. Seifritz E, Di Salle F, Esposito F, et al. Enhancing BOLD response in the auditory system by neurophysiologically tuned fMRI sequence. *Neuroimage.* 2006;29:1013-1022.
43. Wilson EC, Melcher JR, Michey C, et al. Cortical FMRI activation to sequences of tones alternating in frequency: relationship to perceived rate and streaming. *J Neurophysiol.* 2007;97:2230-2238.
44. Shin J, Ahn S, Hu X. Correction for the T1 effect incorporating flip angle estimated by Kalman filter in cardiac-gated functional MRI. *Magn Reson Med.* 2013;70:1626-1633.
45. Beissner F, Deichmann R, Baudrexel S. fMRI of the brainstem using dual-echo EPI. *Neuroimage.* 2011;55:1593-1599.
46. Napadow V, Dhond R, Park K, et al. Time-variant fMRI activity in the brainstem and higher structures in response to acupuncture. *Neuroimage.* 2009;47:289-301.
47. Zhang W-T, Mainero C, Kumar A, et al. Strategies for improving the detection of fMRI activation in trigeminal pathways with cardiac gating. *Neuroimage.* 2006;31:1506-1512.
48. De Martino F, Moerel M, van de Moortele PF, et al. Spatial organization of frequency preference and selectivity in the human inferior colliculus. *Nat Commun.* 2013;4:1386.
49. Moerel M, De Martino F, Ugurbil K, Yacoub E, Formisano E. Processing of frequency and location in human subcortical auditory structures. *Sci Rep.* 2015;5:17048.
50. Denison RN, Vu AT, Yacoub E, et al. Functional mapping of the magnocellular and parvocellular subdivisions of human LGN. *Neuroimage.* 2014;102:358-369.
51. Haynes JD, Deichmann R, Rees G. Eye-specific effects of binocular rivalry in the human lateral geniculate nucleus. *Nature.* 2005;438:496-499.
52. Chandrasekaran B, Kraus N, Wong PC. Human inferior colliculus activity relates to individual differences in spoken language learning. *J Neurophysiol.* 2012;107:1325-1336.
53. Katyal S, Zughni S, Greene C, et al. Topography of covert visual attention in human superior colliculus. *J Neurophysiol.* 2010;104:3074-3083.

How to cite this article: Dewey RS, Hall DA, Plack CJ, Francis ST. Comparison of continuous sampling with active noise cancellation and sparse sampling for cortical and subcortical auditory functional MRI. *Magn Reson Med.* 2021;00:1–12. <https://doi.org/10.1002/mrm.28902>